Available online at www.sciencedirect.com
SCIENCE DIRECT®
Catalysis Today 98 (2004) 345–355
CATALYSIS TODAY
www.elsevier.com/locate/cattod

Periodic forcing of three-way catalyst with diffusion in the washcoat

Petr Kočí[a,c], Milan Kubíček[b,c], Miloš Marek[a,c,*]

[a]Department of Chemical Engineering, Prague Institute of Chemical Technology, Technická 5, CZ-166 28 Prague, Czech Republic
[b]Department of Mathematics, Prague Institute of Chemical Technology, Technická 5, CZ-166 28 Prague, Czech Republic
[c]Center for Nonlinear Dynamics of Chemical and Biological Systems, Prague Institute of Chemical Technology, Technická 5, CZ-166 28 Prague, Czech Republic

Available online 30 September 2004

Abstract

Operation of Pt–Rh/Ce/ γ-Al_2O_3 three-way catalytic converter (TWC) with periodic variations of the inlet oxygen concentration is simulated. A lumped mathematical model with complex microkinetic reaction scheme, surface deposition of reaction components and description of diffusion in the porous washcoat structure is employed. The effects of the forcing frequency and amplitude on the light-off and time-averaged conversions of CO, hydrocarbons (HC) and nitrogen oxides NO_x are studied. The influence of oxygen storage capacity (OSC) and effective diffusivity in the washcoat are also examined. The results are discussed on the basis of computed spatiotemporal concentration patterns in the catalytic washcoat. Earlier light-off (i.e., at lower temperature) and higher time-averaged conversions are observed for the forced TWC in comparison with the TWC operated without oscillations in inlet O_2 concentration. Maximum conversions have been found for the forcing frequencies in the range 1–2 Hz and amplitudes of the oscillations higher than $\pm 10\%$ around the stoichiometric value. The frequency 1 Hz corresponds to typical characteristic times for λ-sensor control of air/fuel ratio (A/F) in the automobile engines.

Keywords: TWC; Catalytic reactor; Exhaust gas conversion; Periodic forcing

1. Introduction

Effects of periodic variation of inlet concentrations and/or flow rates on conversion in heterogeneous catalytic reactors are a well-studied problem [1,2]. Periodic operation may bring an improvement of conversion with respect to steady-state regime, but it can also lead to complex dynamic regimes. If the flow rate and/or inlet concentrations of reactions components are varied periodically and reactions are non-linear (e.g., exhibit ignition-extinction hysteresis) then complex non-stationary regimes exhibiting resonances, quasiperiodic and chaotic regimes can arise [3–5]. The feedback control and/or introduction of the time-delay in the control scheme can have similar effects [6].

Catalytic three-way converters (TWCs) are operated inherently with varying inlet flow rates and variations of inlet concentrations and temperature. Under λ-sensor control, the concentration of oxygen in the exhaust gas oscillates around stoichiometric composition (redox ratio close to 1). In such way simultaneous reduction of nitrogen oxides (NO_x) and oxidation of carbon monoxide and hydrocarbons (HC) are achieved. A large number of papers, both experimental and modelling ones, have been devoted to the problem of CO and HC oxidation and NO_x reduction in catalytic monolith reactors under periodic (forced) operation, cf., e.g., [7–14]. TWC monoliths are often operated under conditions of transport resistance, i.e. external heat and mass transfer to the surface of catalytic washcoat and diffusion within the porous catalytic layer. The effects of heat and mass transport resistance in cyclic operations were studied in [15].

Different types of catalysts, different conditions with possible effects of external mass and heat transfer resistance, diffusion in the washcoat and variable forcing parameters were used in the above studies [7–14]. Thus, even if the number of published experimental and modelling studies is large, general rules on the effects of periodic forcing parameters on the light-off and conversion are difficult to state. The development of mathematical models can help not

* Corresponding author. Tel.: +420 22435 3104; fax: +420 2311 7335.
E-mail address: milos.marek@vscht.cz (M. Marek).

0920-5861/$ – see front matter
doi:10.1016/j.cattod.2004.08.002

Nomenclature

a	density of external surface area ($m^2\ m^{-3}$)
A	relative amplitude of oscillations
c	concentration in the bulk gas (mol m^{-3})
c^s	concentration in the washcoat pores (mol m^{-3})
c_p^g	molar heat capacity of the gas (J $mol^{-1}\ K^{-1}$)
c_p^w	specific heat capacity of the solid (J $kg^{-1}\ K^{-1}$)
D^{eff}	effective diffusion coefficient ($m^2\ s^{-1}$)
f	frequency of oscillations (s^{-1})
ΔH_r	standard reaction enthalpy (J mol^{-1})
J	number of reactions
k	kinetic constant of the reaction (dimension depends on the reaction)
k_c	mass transfer coefficient (m s^{-1})
k_h	heat transfer coefficient (J $m^{-2}\ K^{-1}\ s^{-1}$)
L	concentration of active sites in the washcoat (mol m^{-3})
M	molar weight (kg mol^{-1})
p	pressure (Pa)
r	radial coordinate in the washcoat layer (m)
R	reaction rate (mol $m^{-3}\ s^{-1}$)
R^g	universal gas constant (8.31434 J $mol^{-1}\ K^{-1}$)
t	time (s)
T	temperature of the gas (K)
T^s	temperature of the solid phase (K)
u	space velocity (s^{-1})
X	conversion of the component
y	molar fraction of the component
	Greek letters
δ	thickness of the washcoat layer (m)
ε^g	macroscopic porosity of the reactor
ε^s	porosity of the washcoat
θ	coverage of noble-metal sites (Pt, Rh)
ν	stoichiometric coefficient of the component
ξ	coverage of oxygen storage sites (Ce)
ρ^g	gas density (kg m^{-3})
ρ^s	density of the solid phase (kg m^{-3})
χ	coverage of support sites (alumina)
	Subscripts and superscripts
i	index of the gaseous component
in	inlet
j	index of the reaction
k	index of the component deposited on noble-metal sites (Pt, Rh)
m	index of the component deposited on Ce-sites
NM	noble metals (Pt, Rh)
out	outlet
OSC	oxygen storage capacity (CeO_2)
q	index of the component deposited on support (γ-Al_2O_3)
ref	reference value
s	solid phase (washcoat and support)
SUP	support (γ-Al_2O_3)

only to understand the effects of forcing but also in the design of λ-sensor control strategies. As the inlet concentration variations are fast, a proper mathematical models should use non-stationary kinetics with explicit consideration of surface deposition of reaction components and also consider effects of diffusion within the washcoat layer.

A modelling study of oscillatory feeding for single reaction described by three-step microkinetic scheme (CO oxidation by O_2) in TWC monolith was performed already 10 years ago [16]. Until now mostly pseudo-stationary kinetics extended by oxygen storage sub-model has been used for TWC reactions under transient conditions [17]. Complete and detailed non-stationary kinetics of the reactions in catalytic monolith reactors for automobile exhaust gases with specific storage properties has become available only recently.

Series of dynamic experiments on the non-stationary kinetics of typical reactions on Pt–Rh/Ce/ γ-Al_2O_3 three-way catalyst were performed and published by Hoebink and coworkers [18–21]. The results were discussed and evaluated in the form of detailed microkinetic schema. Transient kinetic parameters for CO, C_2H_4 and C_2H_2 oxidation, oxygen storage and release on cerium oxides and $NO/N_2O/NO_2$ transformation and reduction to N_2 were systematically evaluated. Recent experimental study on periodic forcing of TWC converter was published by Skoglundh et al. [7]. The authors found that periodic O_2 and CO inlet concentration pulses shifted the CO and propene light-off towards lower temperatures.

The experimental and modelling study [22] dealt with CO oxidation in a fixed bed reactor on Pt/ γ-Al_2O_3 with high frequency cycling of CO and O_2 inlet concentrations (up to 10 Hz). The study was also aimed on the effects of diffusion in the catalytic pellets and the development of proper non-stationary kinetic model describing dynamic experimental data. The model used in the study of diffusion effects considered mass balances in the well-mixed gas phase (a CSTR-like approximation) and diffusion and reaction in the flat porous plate of the catalyst with both open sides. The authors used the computed oscillatory carbon dioxide turnover frequency at different positions inside the catalyst for explanation of the effects of cycling on time-averaged conversion. They concluded that the cycling can provide (on average) better ratios of surface concentrations of CO and O in the whole catalyst. Diffusion limitations can promote the reaction rate by providing better CO/O ratios with increasing distance from the outer surface.

The interactions among various reaction intermediates on the catalyst internal surface can be far more complicated in the case of three-way catalyst with CO, hydrocarbons and NO_x being converted with inlet oxygen concentration variations. In the paper [23], the kinetic expressions published in [18–21] were employed in a 2D model of TWC monolith converter. However, the paper is mostly devoted to the development of parallelized algorithm for the

solution of an extensive set of partial differential equations describing the model and gives just a few examples of obtained solutions. The results pointed to the significance of the effects of diffusion in the catalytic washcoat.

In this paper we present the first systematic modelling study of TWC forcing that includes such important effects as: (i) complete microkinetic data for NO_x reduction, oxidation of CO and two different types of hydrocarbons, and oxygen storage; (ii) effects of diffusion in the washcoat. The forcing is realized by a periodic variation of the inlet O_2 concentration. The influence of important control parameters (frequency and amplitude of the inlet O_2 oscillations) and properties of TWC (oxygen storage capacity and effective diffusivity) on the TWC light-off and outlet conversions is examined. We use reaction-transport model of the TWC with well-mixed gas phase (i.e., short monolith or recirculation reactor), similarly such as in [22]. Both external transport and diffusion in the catalytic washcoat are included in the model. Microkinetics with surface deposition of reaction components has been employed, which is necessary for proper description of converter dynamics under transient conditions. We study transient operation of TWC under typical conditions, i.e., for periodic variation of the inlet O_2 concentration with frequency of the order of 1 Hz and amplitude variations of the order 10%.

2. Model

A spatially pseudo-1D, heterogeneous model of Pt/Ce/ γ-Al_2O_3 TWC monolith has been developed. It accounts for a well-mixed bulk gas (i.e., short monolith or recirculation reactor) and a thin layer of porous catalytic washcoat, where diffusion, surface deposition and reactions occur. Due to small thickness of the washcoat layer (typically tens of μm) it may be assumed that no temperature gradients occur within the washcoat [24].

Spatially independent temperature and concentrations are assumed in the well-mixed bulk gas. This is a simplification in the comparison with longer catalytic monolithic reactors commercially employed in automobile industry, where axial temperature and concentration gradients become important. However, the testing of new types of catalytic washcoats is often performed approximately under the conditions of well-mixed reactor — small samples (sections) of the monolith are used in laboratory experiments. Spatially 1D models based on the plug flow with axial heat dispersion, but with semi-empirical kinetics and without considering the diffusion in the washcoat, are widely used in the development of automobile converters (cf., e.g., [14]). The use of the complex, spatially 2D model with plug flow, axial heat dispersion, diffusion in the washcoat and complete microkinetic scheme leads to extensive set of partial differential equations and the computation is excessively time-demanding [23,27]. Thus, the detailed parametric study of forcing is now still not feasible with the more complicated models.

2.1. Balances

The model is represented by the following ordinary and partial differential equations (ODEs and PDEs) — mass balances in the well-mixed bulk gas (1), in the washcoat pores (2) and on the catalyst surface (3)–(5), the combined overall mass and enthalpy balance for the well-mixed bulk gas (6) and the enthalpy balance for the solid phase (7); the appropriate boundary conditions are in the form of Eqs. (8) and (9):

$$\frac{\mathrm{d}c_i(t)}{\mathrm{d}t} = u^{\mathrm{in}}c_i^{\mathrm{in}} - u^{\mathrm{out}}c_i + \frac{k_{\mathrm{c}}a}{\varepsilon^{\mathrm{g}}}(c_i^{\mathrm{s}}|_{r=\delta} - c_i) \tag{1}$$

$$\frac{\partial c_i^{\mathrm{s}}(r,t)}{\partial t} = D_i^{\mathrm{eff}}\frac{\partial^2 c_i^{\mathrm{s}}}{\partial r^2} + \frac{1}{\varepsilon^{\mathrm{s}}}\sum_{j=1}^{J}\nu_{i,j}R_j \tag{2}$$

$$\frac{\partial \theta_k(r,t)}{\partial t} = \frac{1}{L_{\mathrm{NM}}}\sum_{j=1}^{J}\nu_{k,j}R_j \tag{3}$$

$$\frac{\partial \xi_m(r,t)}{\partial t} = \frac{1}{L_{\mathrm{OSC}}}\sum_{j=1}^{J}\nu_{m,j}R_j \tag{4}$$

$$\frac{\partial \chi_q(r,t)}{\partial t} = \frac{1}{L_{\mathrm{SUP}}}\sum_{j=1}^{J}\nu_{q,j}R_j \tag{5}$$

$$\begin{aligned}\frac{\mathrm{d}T(t)}{\mathrm{d}t} &= Tu^{\mathrm{out}} - \frac{T^2}{T^{\mathrm{in}}}u^{\mathrm{in}},\\ u^{\mathrm{out}} &= u^{\mathrm{in}} + \frac{k_{\mathrm{h}}a}{\varepsilon^{\mathrm{g}}c_p^{\mathrm{g,m}}}\frac{R^{\mathrm{g}}(T^{\mathrm{s}}-T)}{p}\end{aligned} \tag{6}$$

$$\begin{aligned}\frac{\mathrm{d}T^{\mathrm{s}}(t)}{\mathrm{d}t} &= \frac{k_{\mathrm{h}}a}{\rho^{\mathrm{s}}c_p^{\mathrm{s}}(1-\varepsilon^{\mathrm{g}})}(T-T^{\mathrm{s}})\\ &\quad - \frac{a}{\rho^{\mathrm{s}}c_p^{\mathrm{s}}(1-\varepsilon^{\mathrm{g}})}\sum_{j=1}^{J}\int_{r=0}^{\delta}\Delta H_j R_j\,\mathrm{d}r\end{aligned} \tag{7}$$

$$D^{\mathrm{eff}}\frac{\partial c_i^{\mathrm{s}}}{\partial r}\bigg|_{r=\delta} = k_{\mathrm{c}}(c_i - c_i^{\mathrm{s}}|_{r=\delta}) \tag{8}$$

$$\frac{\partial c_i^{\mathrm{s}}}{\partial r}\bigg|_{r=0} = 0 \tag{9}$$

Eq. (6) result from the combination of the enthalpy and overall mass balance for the bulk gas under the assumptions of ideal gas, constant pressure and constant molar heat capacity of the gas.

2.2. Reaction kinetics

In the model Eqs. (2)–(5), R_j denote reaction rates defined together with the used microkinetic reaction scheme in Table 1. CO and HC oxidation, oxygen storage and release on the

Table 1
TWC microkinetic scheme used in the model

Number	Reaction step	Kinetic expression
1	$CO + * \rightleftharpoons CO^*$	$R_1 = k_1^f L_{NM} C_{CO} \theta_* - k_1^b L_{NM} \theta_{CO^*}$
2	$O_2 + 2* \rightarrow 2O^*$	$R_2 = k_2 L_{NM} C_{O_2} \theta_*$
3	$CO^* + O^* \rightarrow CO_2 + 2*$	$R_3 = k_3 L_{NM} \theta_{CO^*} \theta_O^*$
4	$CO + O^* \rightleftharpoons OCO^*$	$R_4 = k_4^f L_{NM} C_{CO} \theta_O^* - k_4^b L_{NM} \theta_{OCO}^*$
5	$OCO^* \rightarrow CO_2 + *$	$R_5 = k_6 L_{NM} \theta_{OCO}^*$
6	$O_2 + 2s \rightarrow 2O^s$	$R_6 = k_6 L_{OSC} C_{O_2} \xi_s$
7	$CO^* + O^s \rightarrow CO_2 + * + s$	$R_7 = k_7 L_{NM} \theta_{CO^*} \xi_{O^s}$
8	$CO_2 + \gamma \rightleftharpoons CO_2^\gamma$	$R_8 = k_8^f L_{SUP} C_{CO_2} \chi_\gamma - k_8^b L_{SUP} \chi_{CO_2^\gamma}$
9	$C_2H_2 + * \rightleftharpoons C_2H_2^*$	$R_9 = k_9^f L_{NM} C_{C_2H_2} \theta_* - k_9^b L_{NM} \theta_{C_2H_2^*}$
10	$C_2H_2^* + 2* \rightleftharpoons C_2H_2^{***}$	$R_{10} = k_{10}^f L_{NM} \theta_{C_2H_2^*} \theta_*^2 - k_{10}^b L_{NM} \theta_{C_2H_2^{***}}$
11	$C_2H_2^* + 3O^* \rightarrow 2CO^* + H_2O + 2*$	$R_{11} = k_{11} L_{NM} \theta_{C_2H_2^*} \theta_O^*$
12	$C_2H_2^{***} + 3O^* \rightarrow 2CO^* + H_2O + 4*$	$R_{12} = k_{12} L_{NM} \theta_{C_2H_2^{***}} \theta_O^*$
13	$C_2H_2 + O^* \rightleftharpoons C_2H_2O^*$	$R_{13} = k_{13}^f L_{NM} C_{C_2H_2} \theta_O^* - k_{13}^b L_{NM} \theta_{C_2H_2O^*}$
14	$C_2H_2O^* + 2O^* \rightarrow 2CO^* + H_2O + *$	$R_{14} = k_{14} L_{NM} \theta_{C_2H_2O^*} \theta_O^*$
15	$C_2H_2^* + * + 3O^s \rightarrow 2CO^* + H_2O + 3s$	$R_{15} = k_{15} L_{NM} \theta_{C_2H_2^*} \xi_{O^s}$
16	$C_2H_4 + 2* \rightleftharpoons C_2H_4^{**}$	$R_{16} = k_{16}^f L_{NM} C_{C_2H_4} \theta_*^2 - k_{16}^b L_{NM} \theta_{C_2H_4^{**}}$
17	$C_2H_4^{**} \rightleftharpoons C_2H_4^* + *$	$R_{17} = k_{17}^f L_{NM} \theta_{C_2H_4^{**}} - k_{17}^b L_{NM} \theta_{C_2H_4^*} \theta_*$
18	$C_2H_4^{**} + 6O^* \rightarrow 2CO_2 + 2H_2O + 8*$	$R_{18} = k_{18} L_{NM} \theta_{C_2H_4^{**}} \theta_O^*$
19	$C_2H_4^* + 6O^* \rightarrow 2CO_2 + 2H_2O + 7*$	$R_{19} = k_{19} L_{NM} \theta_{C_2H_4^*} \theta_O^*$
20	$C_2H_4 + O^* \rightleftharpoons C_2H_4O^*$	$R_{20} = k_{20}^f L_{NM} C_{C_2H_4} \theta_O^* - k_{20}^b L_{NM} \theta_{C_2H_4O^*}$
21	$C_2H_4O^* + 5O^* \rightarrow 2CO_2 + 2H_2O + 6*$	$R_{21} = k_{21} L_{NM} \theta_{C_2H_4O^*} \theta_O^*$
22	$NO + * \rightleftharpoons NO^*$	$R_{22} = k_{22}^f L_{NM} C_{NO} \theta_* - k_{22}^b L_{NM} \theta_{NO^*}$
23	$NO^* + * \rightarrow N^* + O^*$	$R_{23} = k_{23} L_{NM} \theta_{NO^*} \theta_*$
24	$NO^* + N^* \rightarrow N_2O^* + *$	$R_{24} = k_{24} L_{NM} \theta_{NO^*} \theta_{N^*}$
25	$N_2O^* \rightarrow N_2O + *$	$R_{25} = k_{25} L_{NM} \theta_{N_2O^*}$
26	$N_2O^* \rightarrow N_2 + O^*$	$R_{26} = k_{26} L_{NM} \theta_{N_2O^*}$
27	$N^* + N^* \rightarrow N_2 + 2*$	$R_{27} = k_{27} L_{NM} \theta_{N^*}^2$
28	$NO + O^* \rightleftharpoons NO_2^*$	$R_{28} = k_{28}^f L_{NM} C_{NO} \theta_O^* - k_{28}^b L_{NM} \theta_{NO_2^*}$
29	$NO_2^* \rightleftharpoons NO_2 + *$	$R_{29} = k_{29}^f L_{NM} \theta_{NO_2^*} - k_{29}^b L_{NM} C_{NO_2} \theta_*$

Numbers 1–8, 9–15, 16–21 and 22–29 represent the reaction subsystems for CO, C_2H_2, C_2H_4 and NO_x, respectively. For values of the kinetic parameters, cf. [18–21] and [23].

Ce-sites and $NO/N_2O/NO_2$ transformation and reduction to N_2 are included. Two types of hydrocarbons are employed in the model to represent the complex HC mixture in exhaust gas — C_2H_2 with lower light-off temperature and C_2H_4 with higher light-off temperature. Consistent microkinetic data are now not available for more often used C_3H_6 and C_3H_8. The reaction scheme and the values of kinetic parameters used in simulations follow from the data given in [18–21,23]. Symbols θ_k, ξ_m and χ_q denote fractions of the related components deposited on the noble metal (∗), cerium (s) and γ-Al_2O_3 (γ) surface sites with the capacities L_{NM}, L_{OSC} and L_{SUP}, respectively (cf. Table 1). In the catalytic washcoat layer $r = 0$ corresponds to the wall and $r = \delta$ means the external surface of the washcoat.

2.3. Diffusion in the washcoat

The actual values of effective diffusion coefficients (D_i^{eff}) in the washcoat layer are known only approximately. Experimental results [25] (with relatively wide confidential interval) and different theoretical models applied to bimodal pore-size distribution of the washcoat (macro- and nano-pores) can give large variations of the D^{eff} value. The temperature dependence of effective diffusion coefficient differs for volume diffusion and Knudsen diffusion. The transport in the washcoat includes the combination of both types of diffusion. If we assume Knudsen diffusion to be dominant, temperature- and component-dependent effective diffusivity can be expressed as

$$D_k^{eff}(T) = D_{ref}^{eff} \sqrt{\frac{T}{T_{ref}}} \sqrt{\frac{M_{ref}}{M_k}} \tag{10}$$

Here T_{ref} is the reference temperature (chosen $T_{ref} = 293$ K), M_{ref} the molar weight of the reference component (chosen C_2H_2) and D_{ref}^{eff} the value of effective diffusion coefficient of the reference component at the reference temperature (model parameter). D_{ref}^{eff} values corresponding to that observed in the experiments [25] have been used in our simulations.

2.4. Oscillations of inlet concentrations

The following equation describes periodic variation of inlet O_2 concentrations:

$$c_{O_2}^{in}(t) = \langle c_{O_2}^{in} \rangle (1 + A\sin 2\pi f t) \quad (11)$$

Here $c_{O_2}^{in}(t)$ denotes oscillating value of the inlet O_2 concentration, A and f are amplitude and frequency of the oscillations, respectively, while $\langle c_{O_2}^{in} \rangle$ is respective time-averaged (mean) value of the inlet concentration. In our simulations the stoichiometric concentration has been used as the mean value of the inlet oxygen concentration (cf. Table 3). Please note that for chosen amplitude A the minimum inlet O_2 concentration is $(1 - A)\langle c_{O_2}^{in} \rangle$ and the maximum is $(1 + A)\langle c_{O_2}^{in} \rangle$.

2.5. Software

A versatile software package for dynamic simulation of interconnected systems of reactors and adsorbers was developed in our laboratory. The package was employed in simulations of different types of non-stationary operated catalytic monolith reactors for conversion of automobile exhaust gases, e.g., converters with selective catalytic reduction of NO_x by hydrocarbons under lean conditions [12], NO_x storage catalysts with lean/rich operation [13,14], reactor–adsorber systems (HC traps) for cold-start [26], complex 2D model of three-way catalyst with diffusion in the washcoat [27] and TWC with a non-uniform spatial distribution of Pt and Rh in multi-layered washcoat [28]. The software was also used for the evaluation of kinetic parameters from experimental data [14]. Model of each considered unit in this software package can be described by a system of PDEs and ODEs. Heat and/or mass exchange among individual units and time-dependent course of inlet variables and parameters can be considered. In the presented model of TWC, the method of lines has been used for the transformation of the system of PDEs (2)–(5) with complete microkinetic scheme (cf. Table 1) to a large system of ODEs. The LSODE [29] implicit integration method for stiff systems with internally generated full Jacobian has been used for dynamic simulations.

3. Results

The developed model has been used in the study of the influence of the amplitude and frequency of oscillatory inlet O_2 concentration on the light-off temperature and time-averaged outlet conversions of CO, hydrocarbons and NO_x. Two model hydrocarbons, C_2H_4 and C_2H_2 were considered. The reaction scheme is given in Table 1, the employed values of model parameters are contained in Table 2, and the inlet gas composition used in the simulations is shown in Table 3.

Table 2
The used values of model parameters

Parameter	Value
u^{in} (s^{-1})	20
δ (μm)	30
ε^s	0.7
ε^g	0.8
a (m^{-1})	4000
c_p^s (J kg^{-1} K^{-1})	750
$c_p^{g,m}$ (J mol^{-1} K^{-1})	30
ρ^s (kg m^{-3})	4000
k_c (m s^{-1})	0.5
k_h (J m^{-2} K^{-1} s^{-1})	500
L_{SUP} (mol m^{-3})	300
L_{OSC} (mol m^{-3})	10– 40
L_{NM} (mol m^{-3})	40
D_{ref}^{eff} (m^2 s^{-1})	5×10^{-7} to 2×10^{-6}

Large differences among the outlet conversions for stationary and oscillating inlet oxygen concentrations may occur in situations where the inlet temperature is close to the light-off temperature. Stabilized outlet CO, NO_x and HC concentrations for such case are shown in Fig. 1. Here the inlet temperature is close to the light-off ($T^{in} = 200\,^{\circ}C$), the washcoat thickness is $\delta = 30\,\mu m$ and the reference effective diffusion coefficient (cf. Eq. (10)) $D_{ref}^{eff} = 1 \times 10^{-6}$ m^2 s^{-1}. We can observe that for the stationary inlet oxygen concentration equal to stoichiometric value ($y_{O_2}^{in} = 0.72\%$) is the conversion of CO approximately 70%, the HC conversion is around 25%, and the NO_x conversion is practically zero. Similar values of outlet conversions are obtained for fast cycling of the oxygen inlet concentrations with the frequency 4 Hz. Here the concentrations within the internal surface of the washcoat cannot follow the rapid changes of concentrations in the gas phase and the conversions are then similar as for the stationary inlet concentrations.

Totally different situation arises when the frequency of the forcing is decreased to 2 and 1 Hz. We can observe in Fig. 1 that when the CO conversion reaches approximately 90%, HC conversion is more than 80% and NO_x conversion is approximately 80%. Hence in this case the light-off already occurred and the conversions are accordingly high. However, we can observe significant differences between the form of the outlet concentration courses. The time course of the outlet concentrations for the forcing frequency 1 Hz is

Table 3
Inlet gas composition (molar fractions) used in the simulations (balance N_2)

Component	y_k^{in}
CO (%)	1.2
C_2H_2 (ppm)	200
C_2H_4 (ppm)	400
NO (ppm)	1000
CO_2 (%)	12
O_2 (%)	0.4– 1.0[a]

[a] Stoichiometric $y_{O_2}^{in} = 0.72\%$.

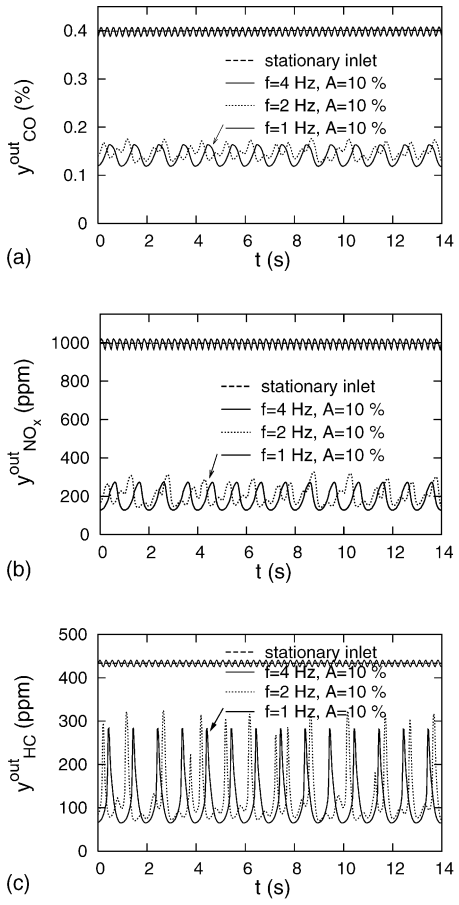

Fig. 1. Comparison of the outlet CO (a), NO_x (b) and HC (c) concentrations for the stationary and oscillating inlet concentration of oxygen with different frequencies (cf. Eq. (11)). Temperature close to the light-off ($T^{in} = 200°C$). $D^{eff}_{ref} = 1 \times 10^{-6}$ m^2 s^{-1}, $L_{OSC} = 20$ mol m^{-3}, $\langle y^{in}_{O_2} \rangle = 0.72\%$ (stoichiometric), inlet concentrations of other components are given in Table 3.

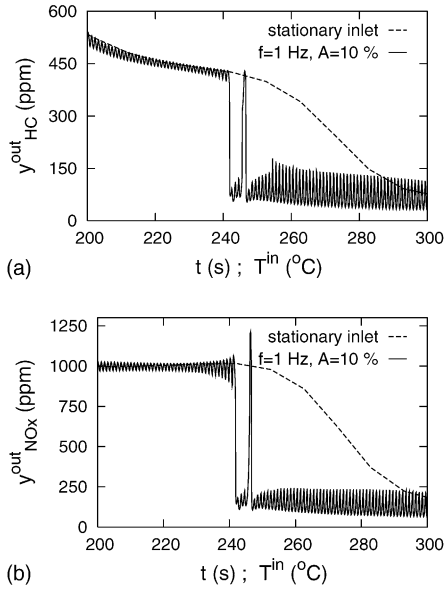

Fig. 2. Comparison of the light-off for the stationary and oscillating inlet concentration of oxygen (cf. Eq. (11)). Evolution of outlet HC (a) and NO_x (b) concentrations is given in the course of temperature ramp 1 K s^{-1}. $D^{eff}_{ref} = 1 \times 10^{-6}$ m^2 s^{-1}, $L_{OSC} = 20$ mol m^{-3}, $\langle y^{in}_{O_2} \rangle = 0.72\%$ (stoichiometric), inlet concentrations of other components are given in Table 3.

periodic and synchronized with the oscillations in the inlet O_2 concentration. Such form of the outlet concentration variations occurs for most values of parameters in the simulations. However, for the forcing frequency 2 Hz the outlet concentration profiles are aperiodic. Generally, they can be either quasiperiodic or chaotic [4,5]. Complex patterns in a periodically forced surface reactions were observed experimentally. For example, for CO oxidation on a Pt single crystals different resonant patterns were observed recently under UHV conditions, ranging from homogeneous oscillations to different irregular spatiotemporal patterns depending on the forcing frequency and amplitude [30]. Complex periodic and chaotic behaviour for the forced CO oxidation on Pt/ γ-Al_2O_3 catalyst under normal pressure was reported earlier [31].

Detailed course of evolution of outlet conversions of hydrocarbons and NO_x for the stationary and oscillating inlet concentration of oxygen when the inlet temperature increases by 1 K s^{-1} (temperature ramp) is represented in Fig. 2. The temperature ramp approximates the situation around the cold-start. The inlet oxygen concentration was varied with the frequency 1 Hz with the amplitude $A = 10\%$ (cf. Eq. (11)). The light-off occurs at temperatures several tens of Kelvin lower and the outlet conversions of hydrocarbons and NO_x then increase fast and reach high values.

The course of mean outlet conversions and actual temperature of the light-off depend both on the frequency and the amplitude of the inlet oscillations. This is illustrated in Fig. 3, where the courses of the mean outlet HC and NO_x concentrations are compared for stationary and oscillating oxygen inlet concentration with the amplitudes 10 and 40%. It can be seen from Fig. 3a that HC adsorption at lower temperatures (T^{in} approximately 0–80 °C) is followed by the desorption peak (T^{in} approximately 130–180 °C) and then the light-off arises. For the stationary inlet concentrations, a two-step HC light-off can be observed in the range of inlet temperatures approximately 200–300 °C (cf. Fig. 3a), as there are two different types of hydrocarbons in the mixture. For the forced operation, the light-off is observed at lower inlet temperatures with faster decrease of mean outlet concentrations. The improvement in the light-off and mean outlet conversions is larger for the higher forcing amplitude.

The results of comprehensive computations of the dependence of the outlet conversions on the frequency and amplitude of the inlet oxygen concentration are summarized for two values of (constant) inlet temperatures in Figs. 4 and 5. The outlet conversions of CO, HC and NO_x are averaged in time after the stabilization of the forced operation at a constant inlet temperature. Thus, the resulting conversions are slightly different from those observed for the

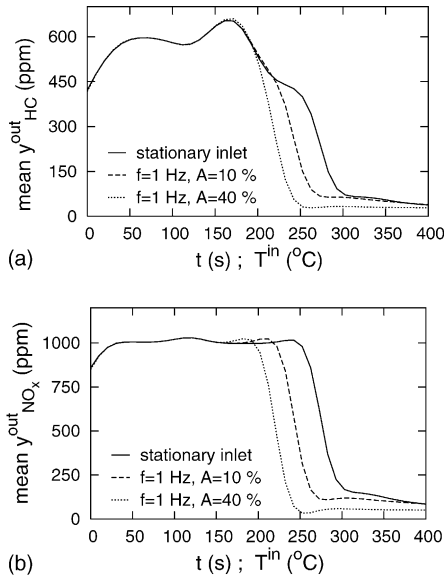

Fig. 3. Dependence of the light-off on the amplitude of oscillations in the inlet oxygen concentration (cf. Eq. (11)). Evolution of mean outlet HC (a) and NO_x (b) concentrations is given in the course of temperature ramp 1 K s^{-1}. $D^{eff}_{ref} = 1 \times 10^{-6}$ m^2 s^{-1}, $L_{OSC} = 20$ mol m^{-3}, $\langle y^{in}_{O_2} \rangle = 0.72\%$ (stoichiometric), inlet concentrations of other components are given in Table 3.

corresponding inlet temperature in the course of temperature ramp (Figs. 2 and 3). The inlet temperature 200 °C (Fig. 4) represents typical behaviour around the light-off. The dependence of outlet conversions on the amplitude of

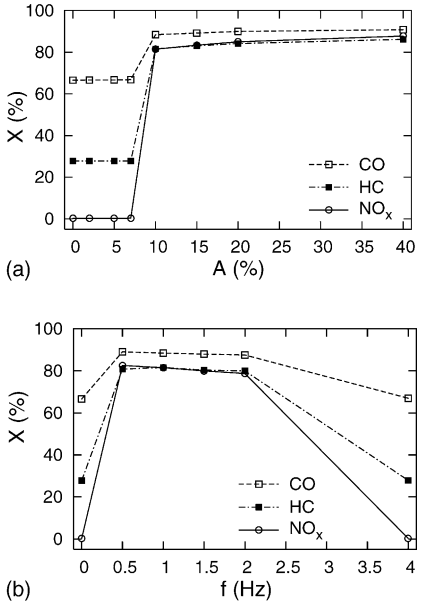

Fig. 4. Time-averaged outlet CO, HC and NO_x conversions in dependence on the amplitude (a) and frequency (b) of oscillations in the inlet concentration of oxygen (cf. Eq. (11)). Temperature close to the light-off ($T_{in} = 200$ °C). $D^{eff}_{ref} = 1 \times 10^{-6}$ m^2 s^{-1}, $L_{OSC} = 20$ mol m^{-3}, $\langle y^{in}_{O_2} \rangle = 0.72\%$ (stoichiometric), inlet concentrations of other components are given in Table 3. (a) Frequency, $f = 1$ Hz; (b) amplitude, $A = 10\%$. Conversions for steady-state inlet conditions can be seen for $A = 0\%$ and $f = 0$ Hz, respectively.

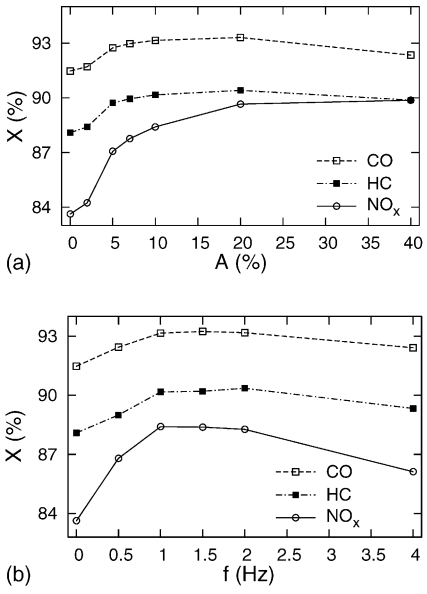

Fig. 5. Time-averaged outlet CO, HC and NO_x conversions in dependence on the amplitude (a) and frequency (b) of oscillations in the inlet concentration of oxygen (cf. Eq. (11)). Temperature close to the light-off ($T_{in} = 200$ °C). $D^{eff}_{ref} = 1 \times 10^{-6}$ m^2 s^{-1}, $L_{OSC} = 20$ mol m^{-3}, $\langle y^{in}_{O_2} \rangle = 0.72\%$ (stoichiometric), inlet concentrations of other components are given in Table 3. (a) Frequency, $f = 1$ Hz; (b) amplitude, $A = 10\%$. Conversions for steady-state inlet conditions can be seen for $A = 0\%$ and $f = 0$ Hz, respectively.

oscillations (Fig. 4a) shows that for the values of forcing amplitudes between 7 and 10% the conversions jump to high values and for higher amplitudes than 10% they stay practically constant. The low values of the forcing amplitude are not sufficient to promote the light-off. The dependence of outlet conversions on the forcing frequency (Fig. 4b) shows that high values of outlet conversions occur for frequencies between 0.5 and 2 Hz. For higher frequencies the conversions sharply decrease, as the concentrations of intermediates at the inner catalyst surface cannot follow the rapid changes of concentrations in the gas phase and the surface concentrations remain similar to those for stationary inlet.

Similar behaviour can be observed after the light-off. This is documented in Fig. 5, where the dependence of outlet conversions on the frequency and amplitude of the inlet oxygen concentrations is shown for the inlet temperature 300 °C. The values for zero amplitude (Fig. 5a) and zero frequency (Fig. 5b) correspond to stationary inlet value of oxygen concentration (stoichiometric $y^{in}_{O_2} = 0.72\%$). The dependence of outlet conversions on the amplitude of inlet O_2 oscillations (Fig. 5a) shows similarly as in Fig. 4a that the conversions increase with the increasing amplitude. However, the increase is just several percents. After the amplitude reaches the value approximately 10%, conversions remain practically at a constant value, with a slight decrease for the amplitudes higher than 20%. The dependence of outlet conversions on the forcing frequency is depicted in Fig. 5b. In the range of frequencies 1–2 Hz

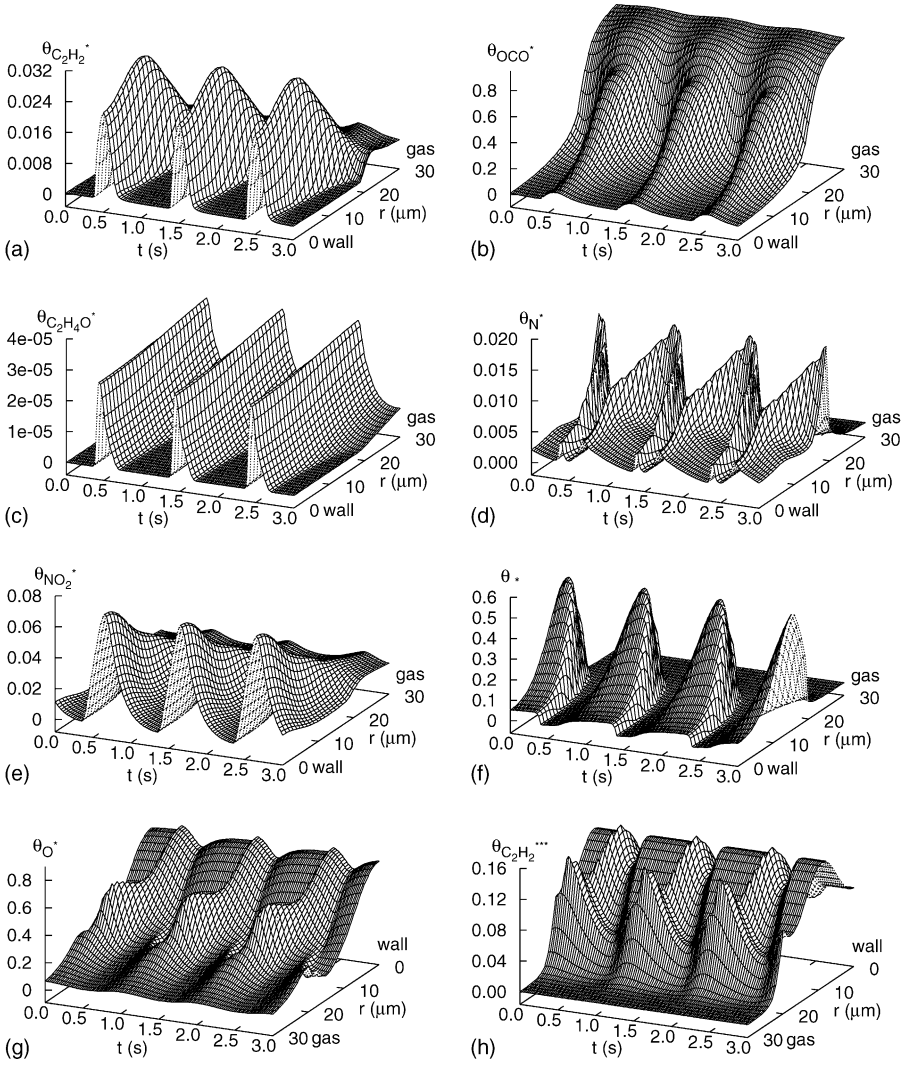

Fig. 6. Spatiotemporal concentration patterns of the species deposited on the noble-metal sites in the washcoat layer. Oscillations in the inlet concentration of oxygen (cf. Eq. (11)). $A = 10\%, f = 1$ Hz, $T_{in} = 200\,^{\circ}$C, $D_{ref}^{eff} = 1 \times 10^{-6}$ m^2 s^{-1}, $L_{OSC} = 20$ mol m^{-3}, $\langle y_{O_2}^{in} \rangle = 0.72\%$ (stoichiometric), inlet concentrations of other components are given in Table 3. The reversal of coordinates in plots (g) and (h) was made because of better observability.

there exists a flat maximum in the outlet conversions (most pronounced for NO_x). The difference between the situations before and after light-off (Figs. 4 and 5, respectively) is that the resulting improvements of conversion in comparison with the stationary case are far lower at higher temperatures.

Typical spatiotemporal patterns of surface concentrations in the forced system at temperature 200 °C are shown in Fig. 6. The frequency of oscillations in the inlet O_2 concentration is 1 Hz with the amplitude 10%. As can be seen from Figs. 1 and 4, this corresponds to the situation after the light-off, where the outlet conversions of hydrocarbons and NO_x are around 80% and the conversion of CO is around 90%. The influence of periodic variation of the inlet O_2 concentration can be clearly observed — the course of all concentration patterns is periodic in time with the synchronized frequency 1 Hz. The benefit of forced operation with varied inlet O_2 concentration can be attributed to periodic regeneration or reconstruction of the surface. Thus, the active noble-metal sites are not blocked by one type of species, hence the inhibition of reactions is prevented. This is the main reason for the earlier light-off when compared to stationary inlet (cf. Figs. 3 and 4). Furthermore, reducing and oxidizing conditions alternate efficiently in the course of the forcing (cf. Table 3 and Eq. (11)) so that both NO_x reduction and CO and HC oxidation take place in the washcoat.

It can be concluded from Fig. 6 that CO and HC oxidation takes place mainly close to the external surface of the washcoat. It follows from the fact that the external part of the washcoat (approximately top 10 μm, $r \in (20, 30)$ μm) is mostly occupied by oxidized OCO^* species (Fig. 6b). Also we can observe relatively increased concentration of reactive $C_2H_2^{***}$ (Fig. 6a) and sufficient availability of O^* (Fig. 6g) in the top sub-layer. Concentrations of oxidized $C_2H_4O^*$ species are also slightly higher close to the external surface (Fig. 6c). On the contrary, NO_x reduction and N_2 formation occur mainly deeper in the washcoat layer.

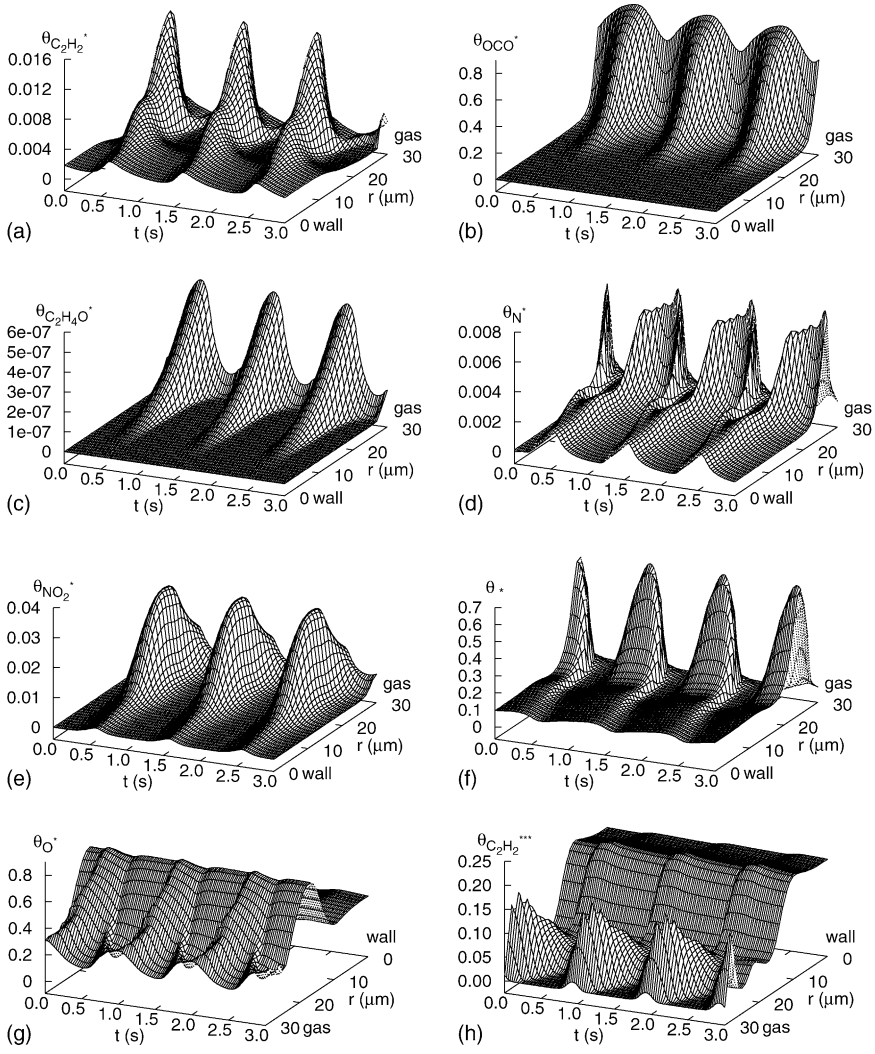

Fig. 7. Spatiotemporal concentration patterns of the species deposited on the noble-metal sites in the washcoat layer. Oscillations in the inlet concentration of oxygen (cf. Eq. (11)). $A = 10\%, f = 1$ Hz, $T_{in} = 300\,^{\circ}C$, $D_{ref}^{eff} = 1 \times 10^{-6}$ m^2 s^{-1}, $L_{OSC} = 20$ mol m^{-3}, $\langle y_{O_2}^{in} \rangle = 0.72\%$ (stoichiometric), inlet concentrations of other components are given in Table 3. The reversal of coordinates in plots (g) and (h) was made because of better observability.

Maximum concentration of the dissociated N* atoms can be seen for $r \in (15, 20)$ μm (Fig. 6d). Also most of the free adsorption sites are in the middle of the washcoat layer (Fig. 6f). Relatively high amount of the strongly adsorbed, non-reactive $C_2H_2^{***}$ is deposited close to the wall (Fig. 6h) together with the unreacted O* (Fig. 6g).

The situation at higher temperature (300 °C) for the same forcing parameters is depicted in Fig. 7. This case corresponds to the state well after the light-off, the stabilized outlet conversions of all components are high. Accordingly there are lower surface concentrations of all reaction intermediates (with the exception of non-reactive $C_2H_2^{***}$ close to the wall) than in the case of lower inlet temperature (compare with Fig. 6). It can be seen that higher surface concentrations of components in Fig. 7 are shifted more to the external washcoat-gas boundary, with steeper concentration gradients. Diffusion limitations become more important with increasing temperature. We can conclude from Fig. 7 that approximately inner 10 μm of the washcoat layer close to the wall ($r \in (0, 10)$ μm) is practically not utilized for the conversion of CO, HC and NO_x under these conditions.

The actual temperature of the light-off in the catalyst parameter space depends critically also on the oxygen storage capacity (L_{OSC}) of the catalyst. Comparison of the time-averaged outlet HC and NO_x conversions for several values of L_{OSC} and different forcing amplitudes is shown in Fig. 8 (temperature close to the light-off). We can infer from the Fig. 8 that the light-off occurs for the highest oxygen storage capacity ($L_{OSC} = 40$ mol m^{-3}) already at zero amplitude (i.e., for the stationary inlet). This means that the Ce-centers in the washcoat exhibit catalytic activity even for non-oscillating conditions (cf. reaction nos. 6, 7 and 15 in Table 1). With the decreasing oxygen storage capacity increasing oscillation amplitudes are necessary to reach the light-off. Typical spatiotemporal concentration pattern of oxygen stored on the Ce-sites (ξ_O^s) for the operation with inlet O_2 forcing is given in Fig. 9. Ce-sites act as the oxygen

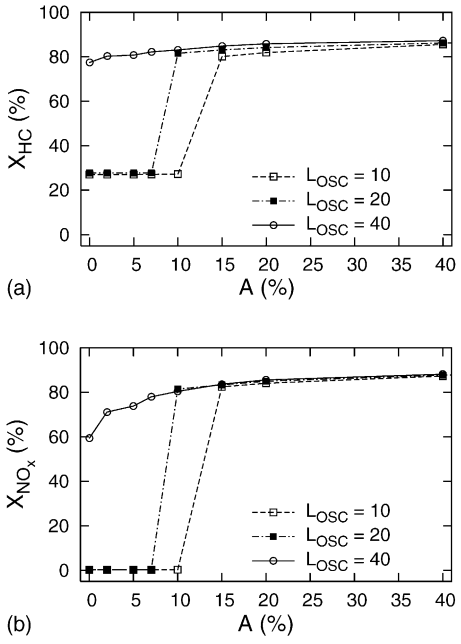

Fig. 8. Comparison of the time-averaged HC (a) and NO_x (b) conversions in the forced TWC with different oxygen storage capacities. Temperature close to the light-off ($T^{in} = 200\,^{\circ}C$). Inlet concentration of oxygen oscillates according to Eq. (11) with frequency $f = 1$ Hz. $D^{eff}_{ref} = 1 \times 10^{-6}$ m^2 s^{-1}, $\langle y^{in}_{O_2} \rangle = 0.72\%$ (stoichiometric), inlet concentrations of other components are given in Table 3.

buffer: O_2 is periodically stored on the surface (reaction no. 6 in Table 1) and released (reaction nos. 7 and 15 in Table 1). The highest concentration of the stored oxygen (and thus the highest Ce activity) can be seen close to the external surface of the washcoat.

Both the light-off and overall time-averaged conversions depend on transport properties in the washcoat, i.e., on the value of effective diffusion coefficient (D^{eff}_{ref}). The evolution of mean outlet CO, NO_x and HC concentrations for three different values of D^{eff}_{ref} and oscillating inlet O_2 concentration in the course of temperature ramp 1 K s^{-1} is shown in Fig. 10. We can observe in Fig. 10a that the mean CO outlet conversion increases with increasing D^{eff}_{ref} for the whole range of inlet temperatures. The mean outlet NO_x and HC

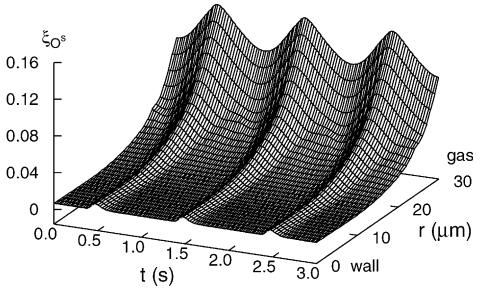

Fig. 9. Spatiotemporal concentration pattern of the oxygen stored on the Ce-sites in the washcoat layer. Oscillations in the inlet concentration of oxygen (cf. Eq. (11)). $A = 20\%$, $f = 1$ Hz, $T_{in} = 200\,^{\circ}C$, $D^{eff}_{ref} = 1 \times 10^{-6}$ m^2 s^{-1}, $L_{OSC} = 10$ mol m^{-3}, $\langle y^{in}_{O_2} \rangle = 0.72\%$ (stoichiometric), inlet concentrations of other components are given in Table 3.

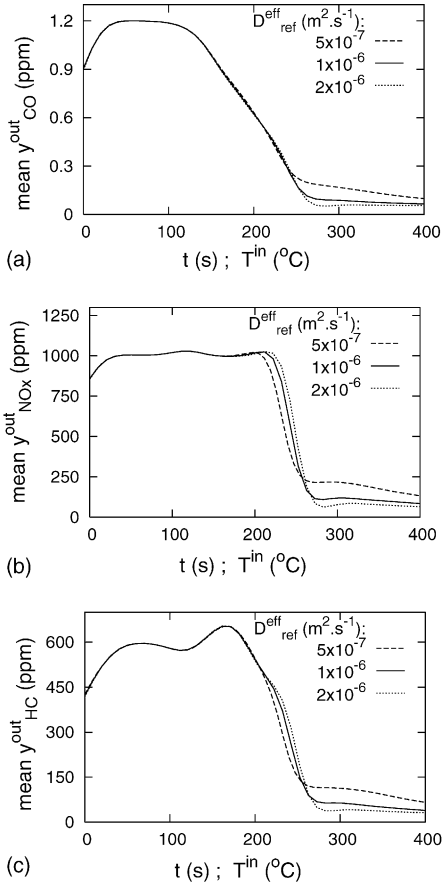

Fig. 10. Comparison of mean outlet CO (a), NO_x (b) and HC (c) concentrations for TWCs with different transport properties of the washcoat (D^{eff}_{ref}). Inlet concentration of oxygen oscillates according to Eq. (11). Temperature ramp 1 K s^{-1}, $A = 10\%$, $f = 1$ Hz, $L_{OSC} = 20$ mol m^{-3}, $\langle y^{in}_{O_2} \rangle = 0.72\%$ (stoichiometric), inlet concentrations of other components are given in Table 3.

conversion (Fig. 10b and c) are in the course of the light-off higher for the catalyst with the lowest value of D^{eff}_{ref}. The non-trivial dependence of the light-off for NO_x and HC follows from the interaction of complex non-linear kinetics and diffusion in the washcoat, which determines the availability of individual species deposited on the noble-metal sites (cf. the spatiotemporal concentration patterns given in Figs. 6 and 7). After the light-off, the NO_x and HC conversions again increase with the increasing D^{eff}_{ref}.

4. Conclusions

Complicated monolith and λ-control design control strategies are being developed to satisfy more stringent regulatory conditions in automotive emissions. They include, for example, combination of close-coupled catalyst operating at high temperature with underfloor catalysts of various composition. Each actual type of the combined converter under lambda sensor control has specific temporal evolution of flow rates, temperature and concentrations of

pollutants. Hence different courses of the time-averaged values of conversions follow. The described software enables to test different strategies of catalyst design and lambda sensor control. The model can be calibrated on experimental data and then used for prediction of the effects of variation of catalyst properties (e.g., oxygen storage capacity or noble-metals distribution within the washcoat) and redox control parameters based on λ-sensor data (frequency and amplitude of oscillations in the inlet concentrations). The predicted behaviour corresponds to the converter with the well-mixed bulk gas, which can be experimentally realized with a short monolith sample or a recycle reactor.

The simulation results described above illustrate the effects of oscillatory inlet oxygen concentration variation on time-averaged conversions and spatiotemporal concentration patterns of reaction intermediates in the washcoat under specific conditions. Resulting time-averaged outlet CO, HC and NO_x conversions for periodic operation are higher than the corresponding steady-state conversions. Furthermore, the model predicts the light-off for oscillating inlet O_2 concentration at lower temperatures than for stationary inlet. This is in good qualitative agreement with experimental observations [7,8]. Generally, the model predicts that under periodic oxygen forcing there exists a window of the forcing amplitudes (usually the amplitude has to be higher than 10%) and forcing frequencies (between 0.5 and 2 Hz) to reach high time-averaged conversions. The knowledge of spatiotemporal concentration patterns of intermediates in the washcoat then enables to determine the effects of diffusion in the washcoat and thus to rationalize its design. The software can be also used to study the effects of general temporal variations of inlet temperature and concentrations of pollutants on the outlet time-averaged conversions. Similar parametric study of TWC forcing based on the use of the spatially 2D model with plug flow and axial heat dispersion will require extensive computing power. We believe that it can be realized in the future.

Acknowledgement

This work has been partially supported by the grants 104/02/0339 and 104/03/H141 of the Czech Grant Agency.

References

[1] P.L. Silveston, R.R. Hudgins, A. Renken, Catal. Today 25 (1995) 91.
[2] P.L. Silveston, Composition Modulation of Catalytic Reactors, Gordon and Breach Science Publishers, Amsterdam, 1998.
[3] J. Řeháček, M. Kubíček, M. Marek, Comput. Chem. Eng. 22 (1998) 283.
[4] M. Marek, I. Schreiber, R. Field, Z. Gyorgyi, Chaos in Chemical and Biochemical Systems, World Scientific, Singapore, 1993, p. 87.
[5] M. Marek, I. Schreiber, Chaotic Behaviour of Deterministic Systems, Cambridge University Press, 1995.
[6] E. Boe, H.C. Chang, Chem. Eng. Sci. 44 (1989) 1281.
[7] M. Skoglundh, P. Thormählen, E. Fridell, F. Hajbolouri, E. Jobson, Chem. Eng. Sci. 54 (1999) 4559.
[8] B.K. Cho, Ind. Eng. Chem. Res. 27 (1988) 30.
[9] P.L. Silveston, Catal. Today 25 (1995) 175.
[10] P.L. Silveston, Can. J. Chem. Eng. 69 (1991) 1106.
[11] R.R. Sadliankar, D.T. Lynch, J. Catal. 149 (1994) 278.
[12] J. Jirát, F. Štěpánek, M. Kubíček, M. Marek, Chem. Eng. Sci. 54 (1999) 2609.
[13] J. Jirát, M. Kubíček, M. Marek, Catal. Today 53 (1999) 583.
[14] P. Kočí, M. Kubíček, M. Marek, T. Maunula, M. Härkönen, Chem. Eng. J. 97 (2004) 131.
[15] J.E. Bailey, F. Horn, R.C. Lin, AIChE J. 17 (1971) 818.
[16] A.B.K. Lie, J. Hoebink, G.B. Marin, Chem. Eng. J. 53 (1993) 47.
[17] D.N. Tsinoglou, G.C. Koltsakis, Chem. Eng. Sci. 58 (2003) 179.
[18] R.H. Nibbelke, A.J.L. Nievergeld, J.H.B.J. Hoebink, G.B. Marin, Appl. Catal. B: Environ. 19 (1998) 245.
[19] J.M. Harmsen, J.H.B.J. Hoebink, J.C. Schouten, Ind. Eng. Chem. Res. 39 (2000) 599.
[20] J.M. Harmsen, J.H.B.J. Hoebink, J.C. Schouten, Chem. Eng. Sci. 56 (2001) 2019.
[21] J.M. Harmsen, J.H.B.J. Hoebink, J.C. Schouten, Catal. Lett. 71 (2001) 81.
[22] J.H.B.J. Hoebink, A.J.L. Nievergeld, G.B. Marin, Chem. Eng. Sci. 54 (1999) 4459.
[23] L.S. Mukadi, R.E. Hayes, Comput. Chem. Eng. 26 (2002) 439.
[24] R. Wanker, H. Raupenstrauch, G. Staudinger, Chem. Eng. Sci. 55 (2000) 4709.
[25] R.E. Hayes, S.T. Kolaczkowski, P.K.C. Li, S. Awdry, Appl. Catal. B: Environ. 25 (2000) 93.
[26] J. Jirát, M. Kubíček, M. Marek, Chem. Eng. Sci. 56 (2001) 1597.
[27] P. Kočí, M. Kubíček, M. Marek, Ind. Eng. Chem. Res. 43 (2004) 4503.
[28] P. Kočí, M. Kubíček, M. Marek, Chem. Eng. Res. Des. 82 (A2) (2004) 284.
[29] A.C. Hindmarsh, in: R.S. Stepleman, et al.(Eds.), ODEpack: A Systematized Collection of ODE Solvers in Scientific Computing, North-Holland, Amsterdam, 1983.
[30] M. Bertram, C. Beta, H.H. Rotermund, G. Ertl, J. Phys. Chem. B 107 (2003) 9610.
[31] M. Marek, L. Rensing, N.I. Jaeger, Temporal Order, Springer-Verlag, Berlin, 1985, p. 105.